

Surface Magnetism in Topological Crystalline Insulators

Sahinur Reja¹, H.A.Fertig¹, L. Brey² and Shixiong Zhang¹

¹Department of Physics, Indiana University, Bloomington, IN 47405

² Instituto de Ciencia de Materiales de Madrid, (CSIC), Cantoblanco, 28049 Madrid, Spain

(Dated: April 2, 2019)

We study a model topological crystalline insulator (TCI) doped with magnetic impurities, in which magnetic ordering at the surface lowers the electronic energy by spontaneous breaking of a crystalline symmetry. This is shown to induce surface ferromagnetism, with favored directions and numbers of energetically equivalent groundstates that are sensitive to the precise density of electrons at the surface. In particular for a (111) surface of a SnTe model in the topological state, magnetic states will have either a two-fold or six-fold symmetry. We compute spin stiffnesses within the model to demonstrate the stability of ferromagnetic states, and consider their ramifications for thermal disordering. Possible experimental consequences of the surface magnetism are discussed.

PACS numbers: 73.20.At, 75.70.Rf, 75.30.Gw

Introduction – Topological crystalline insulators (TCI's) are a class of materials in which the energy bands can host non-trivial topology protected by a crystalline symmetry [1]. These topological bands support surface states [2] which remain gapless provided the crystal symmetry is unbroken, and are believed to present themselves in (Sn,Pb)Te and related alloys [3–8]. Interesting effects may sometimes arise when the symmetry protecting a topological band structure is broken by some perturbation. In topological insulators protected by time-reversal symmetry (TRS), magnetic impurities on a surface may spontaneously order, or form glassy states [9–13]. This can be understood in terms of gap formation of the surface spectrum [14] which would not be possible if the impurity perturbation left TRS intact. By contrast, because TCI's are protected by a crystalline symmetry, the TRS-breaking associated with polarized magnetic impurities does not by itself energetically favor magnetic ordering [15, 16]. However, magnetically ordered states can break the underlying crystalline symmetry [17, 18], gapping the surface state spectrum and potentially favoring the state energetically. In what follows, we explore this physics in a model TCI system.

Our calculations focus on the (111) surface of (Sn,Pb)Te [8, 19–21], using a known model Hamiltonian for the system [3]. Adapting a method developed for TRS topological insulators [22–24], we show how surface states may be projected out from the bulk Hamiltonian, and demonstrate with comparison to tight-binding calculations that these provide a good accounting of the surface states, and in addition allow us to infer the form of the spin operators when projected into these states. The (111) surface states are characterized in this system by four surface Dirac points, one at the $\bar{\Gamma}$ point and one at each of three \bar{M} points [3], and the energy of the first of these is distinct from the others, with interesting consequences. We then consider a model in which the bulk is doped with substitutional isoelectronic magnetic impurities, with the chemical potential adjusted to the bulk gap. The absence of bulk free carriers implies that one does not expect magnetic ordering in the system volume, but

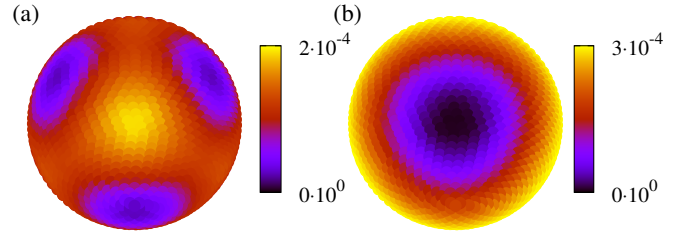


FIG. 1: (Color online.) Total electronic energy per surface atom as a function of magnetization orientation on the Bloch sphere. Color scale is in units of nearest neighbor hopping t . Note that only one hemisphere is shown in each figure, with the \mathbf{k}_1 direction represented by the center. In (a) the Fermi energy is close to $E_{\bar{M}}$; in (b), it is close to $E_{\bar{\Gamma}}$. Results are for fixed particle number.

it can occur on the surface where carriers are present. We find that ferromagnetic orderings which break the mirror symmetry protecting one or more of the surface Dirac points can lead to low energy states, with favored magnetization directions sensitive to the placement of the chemical potential μ , as illustrated in Fig. 1. When in the vicinity of the $\bar{\Gamma}$ point, the groundstates are oriented perpendicular to the surface, and the system represents a ferromagnet with Ising symmetry. When μ is near the \bar{M} point energies, there is a six-fold degenerate set of groundstate orientations, all of which lie closer to the equator of the Bloch sphere. This implies that the magnetization direction can be controlled by a gate near the surface. The existence of these states might be detected experimentally via the behavior of their domain wall excitations – which proliferate at the thermal disordering transitions, or can be present at low temperature when the system is zero-field cooled – and we discuss several potential effects from them in what follows.

Bulk Hamiltonian and Surface States – Our analysis begins with a tight-binding Hamiltonian H_{bulk} for materials in the (Sn,Pb)Te class, which is a rocksalt structure (fcc lattice). H_{bulk} involves twelve orbitals: for each spin there are p_x, p_y, p_z states on each of two sublattices, la-

beled a and b , with on-site energies $m_{a,b}$ (see Supplementary Material [25]). For appropriately chosen parameters, the model is a direct gap semiconductor with smallest gaps at the L points $[\mathbf{k} = \mathbf{k}_1, \mathbf{k}_2, \mathbf{k}_3, \mathbf{k}_4 \equiv (\frac{\pi}{2}, \frac{\pi}{2}, \frac{\pi}{2}), (-\frac{\pi}{2}, \frac{\pi}{2}, \frac{\pi}{2}), (\frac{\pi}{2}, -\frac{\pi}{2}, \frac{\pi}{2}), (\frac{\pi}{2}, \frac{\pi}{2}, -\frac{\pi}{2})$ in units of the inverse nearest neighbor separation]. Its applicability to SnTe has been confirmed by photoemission experiments [26]. For plane-wave states $|\mathbf{k}, \alpha\rangle$ with wavevector \mathbf{k} precisely at an L -point and α all other quantum numbers needed to specify a state, the nearest neighbor hopping integral vanishes so that the states at these points have well-defined sublattice index. Because of this, adjusting $m_b - m_a \equiv m$ continuously allows two states to cross in energy, leading to band inversion and a transition from trivial to topological bands [3]. At an L point, it is possible to explicitly diagonalize H_{bulk} , and for large enough m , the lowest eigenvalue for the b sites are similar to the highest eigenvalue for the a sites, and one can construct a projected 4×4 Hamiltonian representing states with energies in this range which is valid for \mathbf{k} near an L point. (See Supplementary Material [25].) This projected Hamiltonian is conveniently written in terms of states which have well-defined quantum numbers upon $2\pi/3$ rotation around a $\Gamma - L$ direction, denoted as $|1, j\rangle$ for states on the $j = a, b$ sublattice with eigenvalue $e^{-i\pi/3}$, and $|2, j\rangle$ for states with eigenvalue $e^{i\pi/3}$. Projecting H_{bulk} onto the subspace of states of the form $|\ell, j\rangle e^{i\mathbf{k}\cdot\mathbf{q}}$ ($\ell = 1, 2$) with \mathbf{k} at an L point, for small q on finds to quadratic order

$$\begin{aligned} \bar{H}_b = & Aq_3\tau_x - B[q_1\tilde{\sigma}_2 + q_2\tilde{\sigma}_1]\tau_y \\ & + [m + C_{12}^{(-)}(q_1^2 + q_2^2) + C_3^{(-)}q_3^2]\tau_z \\ & + C_{12}^{(+)}(q_1^2 + q_2^2) + C_3^{(+)}q_3^2. \end{aligned} \quad (1)$$

In this expression, $\tilde{\sigma}_1 \equiv \frac{\sqrt{3}}{2}\sigma_x - \frac{1}{2}\sigma_y$ and $\tilde{\sigma}_2 \equiv \frac{\sqrt{3}}{2}\sigma_y + \frac{1}{2}\sigma_x$ are 2×2 matrices acting on the $\ell = 1, 2$ indices of the basis states, and τ_x, τ_y, τ_z are standard Pauli matrices acting on the sublattice index. The A, B , and various C coefficients may be written explicitly in terms of the tight-binding parameters and are presented in detail in the Supplementary Material [25]. Finally, the wavevector coordinate q_3 is along the $\Gamma - L$ direction, while q_1 and q_2 denote directions perpendicular to this. To linear order in q , Eq. 1 is essentially equivalent to previously derived results based on the symmetry of the underlying Hamiltonian [3], but the quadratic terms follow from the microscopic model and play an important role in determining the coupling to surface magnetic degrees of freedom which are the focus of this study. Note that the matrix $\tilde{\sigma}_1$ carries out a mirror reflection which is a symmetry of H_{bulk} ; perturbations which do not spoil this symmetry will result in an effective Hamiltonian near an L point of a similar form [1].

For $m < 0$, on the (111) surface there are gapless surface states [2] located at the four different projections of the L points onto the surface Brillouin zone. These may be constructed individually [22–24], as we describe in the Supplementary Material [25]. Briefly, this involves

searching for eigenstates of the bulk Hamiltonian which are evanescent deep inside the system bulk, and vanish on the surface itself. Focusing on \mathbf{k}_1 , the direction perpendicular to the surface is parameterized by q_3 , so we set $q_1 = q_2 = 0$, $q_3 \rightarrow i\kappa$ in \bar{H}_b to find surface states exactly at the $\bar{\Gamma}$ point. Such an evanescent state must satisfy

$$\left[i\kappa A\tau_x + \left(m - C_3^{(-)}\kappa^2 \right) \tau_z \right] |\kappa\rangle = \left(E + C_3^{(+)}\kappa^2 \right) |\kappa\rangle. \quad (2)$$

Note that arriving at this equation is only possible because we have retained quadratic terms in \bar{H}_b [22–24]. For a given value of E , one finds two values of κ^2 for which Eq. 2 may be satisfied, κ_{\pm}^2 . If $|\kappa_+\rangle \propto |\kappa_-\rangle$, we can form a linear combination that vanishes on the surface. One may show that for $\text{sgn}(mC_3^{(-)}) < 0$, there is a unique value of E for which this is possible, given in this case by $E = E_{\bar{\Gamma}} \equiv -\frac{C_3^{(+)}}{C_3^{(-)}}m$. From Eq. 2 it is clear that there are two independent pairs of $|\kappa_{\pm}\rangle$, which may be characterized by different quantum numbers under $\tilde{\sigma}_3 \equiv -i\tilde{\sigma}_1\tilde{\sigma}_2$. Thus we have two degenerate surface states at the $\bar{\Gamma}$ point, forming a surface Dirac point with energy $E_{\bar{\Gamma}}$ within the bulk gap. The corresponding analysis for the \bar{M} points yields Dirac point energies $E_{\bar{M}} = -m\frac{C_{12}^{(+)}\eta^2 + C_3^{(+)}}{C_{12}^{(-)}\eta^2 + C_3^{(-)}}$, so that $E_{\bar{\Gamma}} \neq E_{\bar{M}}$, in agreement with tight-binding calculations [27]. To simplify subsequent discussion, we drop the particle-hole symmetry-breaking terms ($C_{12}^{(+)}, C_3^{(+)} \rightarrow 0$) in \bar{H}_b , except to note that the surface Dirac point energies at the $\bar{\Gamma}$ and \bar{M} points are different (see Supplementary Material [25]); our resulting surface theories are correct to linear order in wavevector with this approximation.

Magnetic Impurities and Surface Hamiltonians – It has long been known that metals in the (Sn/Pb)Te class [28–36], may be doped with magnetic ions which in some circumstances order ferromagnetically at low temperature. In these systems the magnetic ions enter substitutionally for Sn/Pb atoms, and the coupling of the magnetic moments with the conduction electrons can be understood rather well using an $s-d$ model [37], $H_{sd} = J \sum_i \vec{S}(\mathbf{r}_i) \cdot \vec{s}_i$, where \vec{s}_i represents an impurity spin at location \mathbf{r}_i and $\vec{S}(\mathbf{r}_i)$ is the conduction electron spin density at that location. (Very recently it has been suggested that when ferromagnetically ordered these systems may become Weyl semimetals [38].) In this work we consider the situation where the chemical potential is in a gap of the bulk spectrum, so that free carriers are not present and bulk magnetic ordering is not expected. In the TCI state, however, surface electrons couple the magnetic moments of the substitutional impurities near the surface, and may lead to ferromagnetic ordering. Analogous physics occurs, for example, in graphene [39]. We will model this by assuming magnetic impurities are present in the system, on one sublattice, near the surface.

The explicit surface wavefunctions derived above provides one way to explore this physics, in particular by

allowing us to project the electron spin operators onto surface states for the $\bar{\Gamma}$ and \bar{M} points. As discussed in the Supplementary Material [25], the spin operators on a single (say, the a) sublattice may be written for either the $\bar{\Gamma}$ or an \bar{M} point as

$$\vec{S}^{(a)} = \frac{1}{4} (u_a^2 \tilde{\sigma}_2, u_a^2 \tilde{\sigma}_1, (u_a^2 - v_a^2) \tilde{\sigma}_3). \quad (3)$$

The quantities u_a, v_a are real coefficients involving the tight-binding parameters, with precise definitions provided in the Supplementary Material [25]. Note that the $\tilde{\sigma}_i$ operators act on a different pair of surface states for each of the four surface Dirac points, specifically eigenstates of $\tilde{\sigma}_3$ defined with respect to the relevant Γ - L direction. To further simplify the model, we assume the impurity spins ferromagnetically order and treat the Hamiltonian in mean-field theory; the linear stability of the state against formation of a spin-density wave can then be checked. Projecting H_{sd} onto the subspace of surface states for a Dirac point using Eq. 3 leads to an effective Hamiltonian of the form

$$H_i \approx E_i + \alpha_i(q_2 - b_2)\tilde{\sigma}_1 + \beta_i(q_1 - b_1)\tilde{\sigma}_2 + \Delta_i\tilde{\sigma}_3, \quad (4)$$

where i denotes either $\bar{\Gamma}$ or one of the \bar{M} points, and the relationships between (q_1, q_2) and (q_x, q_y, q_z) depend on the specific Dirac point i . As expected on general symmetry grounds, $\alpha_{\bar{\Gamma}} = \beta_{\bar{\Gamma}}$, but $\alpha_{\bar{M}} \neq \beta_{\bar{M}}$. The offsets b_1 and b_2 are proportional to components of the impurity magnetization perpendicular to \mathbf{k}_i , while Δ is proportional to the component along it. The resulting spectra, $\varepsilon_i = E_i \pm \sqrt{\alpha_i^2(q_1 - b_1)^2 + \beta_i^2(q_2 - b_2)^2 + \Delta_i^2}$, provides the important observation that when the moments align along a Γ - L direction and $\mu \sim E_i$, a gap opens in the corresponding surface spectrum that lowers its contribution to the total electron energy [14].

Numerical Studies – To test this idea we have numerically computed the electronic energy of a TCI slab with open (111) surfaces, using the tight-binding model H_{bulk} [25] as our Hamiltonian, and adding an effective magnetic field \vec{b} near the surface on only the a sublattice, in such a way that their coupling to the two states associated with the surface Dirac cones is the same. Our tight-binding parameters are adapted from Ref. 40, and we have verified the presence of four surface Dirac points at the $\bar{\Gamma}$ point when no magnetization is present. Initially we consider a slab with primitive unit cell presenting only a single site of one sublattice on the surface, and introduce a surface magnetization as described above. While this represents a relatively large density of impurities, it captures the correct qualitative physics, and allows us to study a wide enough slab that the surfaces are effectively decoupled. As expected from the above discussion, among the four the Dirac cones the one with largest magnetization projection along its corresponding Γ - L direction develops the largest gap. Fig. 1 illustrates the resulting total electronic energy for two different scales of Fermi energy as a function of the magnetic orientation.

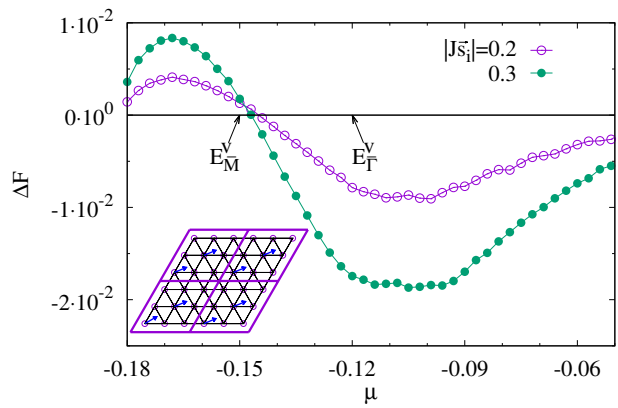


FIG. 2: (Color online.) Difference in free energy per surface atom in units of nearest neighbor hopping t , when magnetic moments are oriented in the (111) direction and in the $(11\bar{1})$ direction, as a function of chemical potential, for two different strengths of $J|\vec{s}|$ in H_{sd} . $E_{\bar{\Gamma}}^V$ and $E_{\bar{M}}^V$ indicate valence band tops for $J|\vec{s}| = 0.3$ with \vec{s} in each direction respectively. Here there are 2 magnetic ions for 9 atoms on the surface in the unit cell (inset).

Panels (a) and (b) show results for particle numbers such that the Fermi energy is near $E_{\bar{M}}$ and $E_{\bar{\Gamma}}$ respectively in the absence of magnetic impurities. With them present, the energy is minimized in the former case for \vec{s} along a Γ - L direction associated with an \bar{M} point, while in the latter minimization occurs for \vec{s} along \mathbf{k}_1 . Thus in the $\mu \sim E_{\bar{\Gamma}}$ case one finds two (equal) energy minima on the Bloch sphere, while for $\mu \sim E_{\bar{M}}$ there are six. (Only half of these can be seen in the figures.) Analogous results are found when the chemical potential rather than particle number is fixed. As expected from the above analysis, minimal energy directions are picked out by the orientations that maximize gap openings near the Fermi energy.

To further substantiate this, we also studied a more dilute magnetic moment model, in which the impurities are present only for 2/9 of the atoms of one sublattice near the surface, as illustrated in the inset of Fig. 2. The main panel shows the difference in Gibbs free energy of the system ($\langle H_{bulk} \rangle - \mu N$ with N the number of electrons) when the magnetic moments are oriented in the (111) direction and in the $(11\bar{1})$ direction, as a function of chemical potential. The results again demonstrate that energetically favored directions are determined by μ . We have also used this geometry to verify that orienting the two surface magnetic moments in different directions always raises the energy of the system, supporting our assumed ferromagnetic ordering.

The ferromagnetic ordering may be further substantiated by considering what happens to the electronic energy when the effective field is allowed to vary spatially with some wavevector \vec{Q} along an average direction, $b_{1,2}(\mathbf{r}) = b_{1,2}^{(0)} + \delta b_{1,2} \cos(i\mathbf{Q} \cdot \mathbf{r})$, $\Delta(\mathbf{r}) \equiv \Delta^{(0)} + \delta\Delta \cos(i\mathbf{Q} \cdot \mathbf{r})$. To compute this we adopt as our basic

Hamiltonian Eq. 4, assuming for simplicity $\alpha_i = \beta_i \equiv \alpha$, use the directions associated with q_1 and q_2 to define x and y directions on the surface, and compute the change in energy to second order in $\delta b_{1,2}$, $\delta\Delta$, and Q . Interestingly, for the valleys in which there are Fermi surfaces, this turns out to be independent of Q , as is the case for graphene [39]. Thus the spin stiffness (quadratic dependence of the energy correction on Q) comes from any valley(s) for which the Fermi energy passes through a gap. After an involved calculation (see Supplementary Material [25]), one finds a correction of the form

$$\frac{\delta E(Q) - \delta E(0)}{\mathcal{S}} = \frac{1}{2} \sum_{\mu, \nu=x,y} \rho_{\mu,\nu} Q_\mu Q_\nu, \quad (5)$$

where the coefficients $\rho_{\mu,\nu}$ are all second order in the deviations $\delta b_{1,2}$, $\delta\Delta$, and the eigenvalues of the 2×2 matrix it represents are positive [41]. This demonstrates that if the effective field from the surface magnetization has a spatial oscillation, the resulting energy increases with increasing oscillation wavevector, as should be for a ferromagnetically aligned groundstate. A notable property of the stiffnesses $\rho_{\mu,\nu}$ is that they all diverge as $1/\Delta^{(0)}$ [25]; we return to this point in the next section.

Discussion and Speculations – We next consider some physical consequences of the surface magnetism discussed above, focusing on temperature ranges where the impurity magnetic moments may be treated classically. As remarked upon above, the sensitivity of the low-energy directions of the magnetization to the chemical potential should allow it to be controlled via a gate potential, which in principle would be observable in direct magnetization measurements. Another basic observation is that the gap openings induce a Berry’s curvature in the surface bands, which generically induces an anomalous Hall effect. For this system we do not expect it to be quantized [17, 18], since the chemical potential typically cannot pass through a gap for all the surface Dirac species at the same time.

It is interesting to consider possible consequences of $\rho_{\mu\nu} \sim 1/\Delta^{(0)}$ as discussed above. In particular we expect that the multiple minima presented in Fig. 1 imply that there should be domain wall (DW) excitations in the system, with energy per unit length scaling as $\sqrt{\Delta^{(0)}\rho_0}$, with ρ_0 an appropriate average of $\rho_{\mu\nu}$ ’s. This remains *finite* even as $\Delta^{(0)}$ vanishes, as should happen at high enough temperature. The divergence of the spin stiffness, $\rho_0 \sim 1/\Delta^{(0)}$, reflects the fact that as the gap vanishes, the quantity $\delta E(\mathbf{Q})$ is no longer analytic in \mathbf{Q} , and in particular rises *linearly* with Q in the long wavelength limit [39], suggesting a non-local interaction among spin gradients. Presuming μ ends up at the Dirac point as $\Delta^{(0)}$ vanishes, the simplest model of the system is a clock model with long-range interactions, which in the Ising case would approach the transition with mean-field exponents [42]. For other values of μ it is possible that DW’s with finite energy per unit length can be stabilized

in this circumstance, but if so would not have the simplest structure [43]. In this situation, for the $\mu \sim E_{\bar{\Gamma}}$ case [cf. Fig. 1(a)], the system presumably will undergo a second order phase transition in the Ising universality class. In the $\mu \sim E_{\bar{M}}$ case [Fig. 1(b)], with six different minima one expects that a simpler theory with the same long-wavelength physics will be a six-state clock model. In this case, the phase transition is known to be in the Kosterlitz-Thouless universality class [44].

We also note that DW excitations in this system may accumulate charge, both due to mid-gap states [45, 46], as well as from the surface valleys which have Fermi surfaces allowing low-energy scattering. At the critical temperature T_c where the transition occurs, one expects DW’s to proliferate, opening a channel for conduction which is absent below T_c . This could lead to singular behavior (e.g., a cusp) in the conductivity of the surface at the transition [47, 48], and should also have a signature when the surface is probed via tunneling. A further possibility is to probe the system by looking for differences in surface conduction when the system is field-cooled through its critical temperature from when it is zero field-cooled. The latter leads to nucleation of groundstate domains with random orientation, and DW’s between them, which cannot relax on the time scale of an experiment. Thus one expects stronger surface conduction from a zero field-cooled sample [16, 49, 50].

Finally, the presence of charged DW’s on the surface might be detected directly via coupling to electromagnetic waves [51]. One interesting possibility is to probe diffuse scattering in reflectance from the surface, which should be sensitive to DW proliferation because of the charge associated with them. In a simple model we can associate charge with gradients of the spin parallel to the ordering axis, which in the $\bar{\Gamma}$ case would be the surface normal \hat{z} . Assuming the scattering amplitude is proportional to the charge density leads to an amplitude $A_{\vec{q}} \sim \hat{z} \cdot \vec{\mathcal{E}} \times \mathbf{q} s_z(\mathbf{q})$, where $\vec{\mathcal{E}}$ is the electric field of the light, for plane waves scattered by a wavevector \vec{q} away from the in-plane component of the incident direction. The scattering intensity then reveals information about $\chi = \langle s_z(-\vec{q}) s_z(\vec{q}) \rangle$ which in principle will allow one to identify the universality class of the transition.

In summary, the surface of a magnetically-doped TCI hosts magnetic ordering in the topological state even when the bulk is disordered. The unique electronic structure of a TCI surface leads to a richer set of possible ordered states than would be expected from time-reversal symmetry protected topological insulators, and implies a number of unusual physical behaviors.

Acknowledgements – The authors thank Fernando de Juan for helpful comments, and U. Nitzsche for technical assistance. This work was supported by the NSF through Grant Nos. DMR-1506263 and DMR-1506460, by the US-Israel Binational Science Foundation, and by MEyC-Spain under grant FIS2015-64654-P. Computations were carried out on the ITF/IFW and IU Karst clusters.

-
- [1] L. Fu, Phys. Rev. Lett. **106**, 106802 (2011).
- [2] J. Liu, W. Duan, and L. Fu, Phys. Rev. B **88**, 241303(R) (2013).
- [3] T. Hsieh, H. Lin, J. Liu, W. Duan, and L. Fu, Nat. Commun. **3**, 982 (2012).
- [4] Y. Tanaka and et al., Nat. Phys. **8**, 800 (2012).
- [5] S. Xu and et al., Nat. Phys. **3**, 1192 (2012).
- [6] P. Dziawa and et al., Nat. Comm. **11**, 1023 (2012).
- [7] Y. Okada and et al., Science **341**, 6153 (2013).
- [8] C. Yan and et al., Phys. Rev. Lett. **112**, 186801 (2014).
- [9] A. Liu, C. Liu, C. Xu, X. Qu, and S. Zhang, Phys. Rev. Lett. **102**, 156603 (2009).
- [10] R. R. Biswas and A. V. Balatsky, Phys. Rev. B **81**, 233405 (2010), URL <http://link.aps.org/doi/10.1103/PhysRevB.81.233405>.
- [11] I. Garate and M. Franz, Phys. Rev. B **81**, 172408 (2010), URL <http://link.aps.org/doi/10.1103/PhysRevB.81.172408>.
- [12] D. Abanin and D. Pesin, Phys. Rev. Lett. **106**, 136802 (2011).
- [13] C.-X. Liu, B. Roy, and J. D. Sau, Phys. Rev. B **94**, 235421 (2016), URL <http://link.aps.org/doi/10.1103/PhysRevB.94.235421>.
- [14] D. Efimkin and V. Galitski, Phys. Rev. B **89**, 115431 (2014).
- [15] J. Shen and J. J. Cha, Nanoscale **6**, 14133 (2014).
- [16] B. A. Assaf, F. Katmis, P. Wei, C.-Z. Chang, B. Satpati, J. S. Moodera, and D. Heiman, Phys. Rev. B **91**, 195310 (2015), URL <http://link.aps.org/doi/10.1103/PhysRevB.91.195310>.
- [17] F. Zhang, X. Li, J. Feng, C. Kane, and E. Mele, arXiv:1309.7682.
- [18] C. Fang, M. J. Gilbert, and B. A. Bernevig, Phys. Rev. Lett. **112**, 046801 (2014), URL <https://link.aps.org/doi/10.1103/PhysRevLett.112.046801>.
- [19] Z. Li, S. Shao, N. Li, K. McCall, J. Wang, and S. X. Zhang, Nano Letters **13**, 5443 (2013).
- [20] A. A. Taskin, F. Yang, S. Sasaki, K. Segawa, and Y. Ando, Phys. Rev. B **89**, 121302 (2014), URL <http://link.aps.org/doi/10.1103/PhysRevB.89.121302>.
- [21] J. Shen, Y. Jung, A. S. Disa, F. J. Walker, C. H. Ahn, and J. J. Cha, Nano Letters **14**, 4183 (2014).
- [22] C.-X. Liu, X.-L. Qi, H. Zhang, X. Dai, Z. Fang, and S.-C. Zhang, Phys. Rev. B **82**, 045122 (2010), URL <https://link.aps.org/doi/10.1103/PhysRevB.82.045122>.
- [23] P. G. Silvestrov, P. W. Brouwer, and E. G. Mishchenko, Phys. Rev. B **86**, 075302 (2012), URL <http://link.aps.org/doi/10.1103/PhysRevB.86.075302>.
- [24] L. Brey and H. A. Fertig, Phys. Rev. B **89**, 084305 (2014).
- [25] See Online Supplementary Material.
- [26] P. Littlewood and et al., Phys. Rev. Lett. **105**, 086404 (2010).
- [27] C. Polley and et al., Phys. Rev. B **89**, 075317 (2014).
- [28] M. Inoue, K. Ishii, and T. Tatsukawa, J. Low Temp. Phys. **23**, 785 (1975).
- [29] M. Inoue, K. Ishii, and H. Yagi, J. Phys. Soc. Japan **43**, 903 (1977).
- [30] M. Inoue, T. Tanabe, H. Yagi, and T. Tatsukawa, J. Phys. Soc. Japan **47**, 1879 (1979).
- [31] T. Story, R. R. Galazka, R. B. Frankel, and P. A. Wolff, Phys. Rev. Lett. **56**, 777 (1986), URL <http://link.aps.org/doi/10.1103/PhysRevLett.56.777>.
- [32] G. Karczewski, J. K. Furdyna, D. L. Partin, C. N. Thrush, and J. P. Heremans, Phys. Rev. B **46**, 13331 (1992), URL <http://link.aps.org/doi/10.1103/PhysRevB.46.13331>.
- [33] F. Geist, H. Pascher, N. Frank, and G. Bauer, Phys. Rev. B **53**, 3820 (1996), URL <http://link.aps.org/doi/10.1103/PhysRevB.53.3820>.
- [34] F. Geist, W. Herbst, C. Mejía-García, H. Pascher, R. Rupprecht, Y. Ueta, G. Springholz, G. Bauer, and M. Tacke, Phys. Rev. B **56**, 13042 (1997), URL <http://link.aps.org/doi/10.1103/PhysRevB.56.13042>.
- [35] A. Prinz, G. Brunthaler, Y. Ueta, G. Springholz, G. Bauer, G. Grabecki, and T. Dietl, Phys. Rev. B **59**, 12983 (1999), URL <http://link.aps.org/doi/10.1103/PhysRevB.59.12983>.
- [36] A. Łusakowski, A. Jędrzejczak, M. Górska, V. Osinniy, M. Arciszewska, W. Dobrowolski, V. Domukhovski, B. Witkowska, T. Story, and R. R. Galazka, Phys. Rev. B **65**, 165206 (2002), URL <http://link.aps.org/doi/10.1103/PhysRevB.65.165206>.
- [37] T. Dietl, C. Śliwa, G. Bauer, and H. Pascher, Phys. Rev. B **49**, 2230 (1994), URL <http://link.aps.org/doi/10.1103/PhysRevB.49.2230>.
- [38] J. Liu, C. Fang, and L. Fu, arXiv:1604.03947 (2016).
- [39] L. Brey, H. A. Fertig, and S. Das Sarma, Phys. Rev. Lett. **99**, 116802 (2007), URL <http://link.aps.org/doi/10.1103/PhysRevLett.99.116802>.
- [40] I. Fulga, N. Avraham, H. Beidenkopf, and A. Stern, Phys. Rev. B **94**, 125405 (2016).
- [41] Precise results for the stiffnesses are provided in the Supplementary Material.
- [42] M. F. Paulos, S. Rychkov, B. C. van Rees, and B. Zan, Nuc. Phys. B **902**, 246 (2016).
- [43] R. Rajaraman, *Solitons and Instantons* (North-Holland, New York, 1989).
- [44] J. V. José, L. P. Kadanoff, S. Kirkpatrick, and D. R. Nelson, Phys. Rev. B **16**, 1217 (1977), URL <http://link.aps.org/doi/10.1103/PhysRevB.16.1217>.
- [45] R. Jackiw and C. Rebbi, Phys. Rev. D **13**, 3398 (1976).
- [46] A. Schaakel, *Boulevard of Broken Symmetries* (World Scientific, 2008).
- [47] T. Jungwirth and A. H. MacDonald, Phys. Rev. Lett. **87**, 216801 (2001), URL <http://link.aps.org/doi/10.1103/PhysRevLett.87.216801>.
- [48] K. Dhochak, E. Shimshoni, and E. Berg, Phys. Rev. B **91**, 165107 (2015), URL <http://link.aps.org/doi/10.1103/PhysRevB.91.165107>.
- [49] K. Ueda, J. Fujioka, B.-J. Yang, J. Shiogai, A. Tsukazaki, S. Nakamura, S. Awaji, N. Nagaosa, and Y. Tokura, Phys. Rev. Lett. **115**, 056402 (2015), URL <http://link.aps.org/doi/10.1103/PhysRevLett.115.056402>.
- [50] Z. Tian and et al., Nat. Phys. **12**, 134 (2016).
- [51] E. Y. Ma, Y.-T. Cui, K. Ueda, S. Tang, K. Chen, N. Tamura, P. M. Wu, J. Fujioka, Y. Tokura, and Z.-X. Shen, Science **350**, 538 (2015), ISSN 0036-8075, <http://science.sciencemag.org/content/350/6260/538.full.pdf>, URL <http://science.sciencemag.org/content/350/6260/538>.

Supplementary information for “Surface Magnetism in Topological Crystalline Insulators”

Sahinur Reja¹, H.A.Fertig¹, L. Brey² and Shixiong Zhang¹

¹Department of Physics, Indiana University, Bloomington, IN 47405

² Instituto de Ciencia de Materiales de Madrid, (CSIC), Cantoblanco, 28049 Madrid, Spain

I. BULK HAMILTONIAN

Our analysis begins with a tight-binding model [1] for materials in the (Sn,Pb)Te class, which is a rocksalt

structure, i.e. an fcc lattice with a two sublattices, such that atomic species alternate among the points of a simple cubic lattice. The Hamiltonian of the system is given by $H_{bulk} = H_m + H_{nn} + H_{nnn} + H_{so}$, with

$$\begin{aligned} H_m &= \sum_j m_j \sum_{\mathbf{R},s} \vec{c}_{j,s}^\dagger(\mathbf{R}) \cdot \vec{c}_{j,s}(\mathbf{R}), \\ H_{nn} &= t \sum_{(\mathbf{R},\mathbf{R}'),s} \vec{c}_{a,s}^\dagger(\mathbf{R}) \cdot \vec{d}_{\mathbf{R},\mathbf{R}'} \vec{d}_{\mathbf{R},\mathbf{R}'} \cdot \vec{c}_{b,s}(\mathbf{R}') + h.c., \\ H_{nnn} &= \sum_j t'_j \sum_{((\mathbf{R},\mathbf{R}'),s)} \vec{c}_{j,s}^\dagger(\mathbf{R}) \cdot \vec{d}_{\mathbf{R},\mathbf{R}'} \vec{d}_{\mathbf{R},\mathbf{R}'} \cdot \vec{c}_{j,s}(\mathbf{R}') + h.c., \\ H_{so} &= i \sum_j \lambda_j \sum_{\mathbf{R},s,s'} \vec{c}_{j,s}^\dagger(\mathbf{R}) \times \vec{c}_{j,s'}(\mathbf{R}) \cdot (\vec{\sigma})_{s,s'}. \end{aligned} \quad (S1)$$

In these equations \mathbf{R} labels the sites of a cubic lattice, $j = a, b$ are the species type (Sn/Pb or Te), which have on-site energies $m_{a,b}$, and $s = \uparrow, \downarrow$ is the electron spin. The 3-vector of operators $\vec{c}_{j,s}(\mathbf{R})$ annihilates electrons in p_x , p_y and p_z orbitals, and there is a local spin-orbit coupling strength λ_j on each site. ($\vec{\sigma}$ is the vector of Pauli matrices.) The vectors $\vec{d}_{\mathbf{R},\mathbf{R}'}$ are unit vectors pointing from \mathbf{R} and \mathbf{R}' , and, finally, the sum over $(\mathbf{R}, \mathbf{R}')$ denotes positions which are nearest neighbors, while $((\mathbf{R}, \mathbf{R}'))$ denotes next nearest neighbors.

At an L point, it is possible to diagonalize H_{bulk} analytically. These eigenvalues are $E_{0,j} = 4t'_j - \lambda_j + m_j$, $E_{\pm,j} = -2t'_j + \lambda_j/2 \pm R_j + m_j$, with $R_j \equiv \sqrt{144t_j'^2 + 24t'_j\lambda_j + 9\lambda_j^2}/2$, with $j = a, b$ each of these three values being doubly degenerate. For large enough m , the lowest eigenvalue for the b sites approaches the highest eigenvalue for the a sites, and we can construct a projected 4×4 Hamiltonian representing states with energies $E \sim E_{+,a} \sim E_{-,b}$ which is valid for \mathbf{k} near an L point. This projected Hamiltonian is conveniently written in terms of states which have well-defined quantum numbers upon $2\pi/3$ rotation around a $\Gamma - L$ direction. For example, for the L point $\mathbf{k}_1 \equiv (\frac{\pi}{2}, \frac{\pi}{2}, \frac{\pi}{2})$, we define states

$$|m, s, j\rangle \equiv \frac{1}{\sqrt{3}} \left[|p_x, j\rangle + w^m |p_y, j\rangle + w^{2m} |p_z, j\rangle \right] \otimes |s\rangle$$

where $|p_x(y,z), j\rangle$ is a $p_x(y,z)$ -orbital on a site of type j , $|s = \pm\rangle$ is a spin state with quantization axis parallel to \mathbf{k}_1 , and $w = e^{2\pi i/3}$. The relevant eigenstates of the Hamiltonian are then

$$\begin{aligned} |1, j\rangle &= -u_j w |m=0, s=+, j\rangle + v_j |m=2, s=-, j\rangle, \\ |2, j\rangle &= u_j w^* |m=0, s=-, j\rangle + v_j |m=1, s=+, j\rangle, \end{aligned} \quad (S2)$$

with

$$\begin{aligned} u_j &= \frac{\sqrt{2}\lambda_j}{\sqrt{(8t'_j + \varepsilon_j)^2 + 2\lambda_j^2}}, \\ v_j &= \frac{8t'_j + \varepsilon_j}{\sqrt{(8t'_j + \varepsilon_j)^2 + 2\lambda_j^2}}, \end{aligned} \quad (S3)$$

$\varepsilon_a = -2t'_a + \lambda_a/2 + R_a$, and $\varepsilon_b = -2t'_b + \lambda_b/2 - R_b$. Note under a $2\pi/3$ rotation around the (111) direction, $|1, j\rangle \rightarrow e^{-i\pi/3} |1, j\rangle$ and $|2, j\rangle \rightarrow e^{i\pi/3} |2, j\rangle$.

To proceed, we form the \mathbf{k} -dependent bulk Hamiltonian $H_b(\mathbf{k}) = e^{-i\mathbf{k}\cdot\mathbf{R}} H_{bulk} e^{i\mathbf{k}\cdot\mathbf{R}}$ which acts on states of definite crystal momentum \mathbf{k} , and project this into the 4×4 space defined by the states in Eq. S2. Writing $\mathbf{k} = \mathbf{k}_1 + \mathbf{q}$, for small q one finds, after considerable algebra and up to an overall constant,

$$\bar{H}_1 = Aq_3\tau_x - B[q_1\tilde{\sigma}_2 + q_2\tilde{\sigma}_1]\tau_y + [m + C_{12}^{(-)}(q_1^2 + q_2^2) + C_3^{(-)}q_3^2]\tau_z + C_{12}^{(+)}(q_1^2 + q_2^2) + C_3^{(+)}q_3^2. \quad (\text{S4})$$

In this expression, $\tilde{\sigma}_1 \equiv \frac{\sqrt{3}}{2}\sigma_x - \frac{1}{2}\sigma_y$ and $\tilde{\sigma}_2 \equiv \frac{\sqrt{3}}{2}\sigma_y + \frac{1}{2}\sigma_x$ are 2×2 matrices acting on the 1,2 indices of the basis states (Eq. S2), and τ_x, τ_y, τ_z are standard Pauli matrices acting on the sublattice index. The coefficients in Eq. S4 are explicitly given by $A = -2\sqrt{3}(u_a u_b + v_a v_b)$, $B = \sqrt{6}(-u_a v_b + v_a u_b)$, $C_{12}^{(\pm)} = \frac{1}{2}[(C_a - D_a/2) \pm (C_b - D_b/2)]$, and $C_3^{(\pm)} = -\frac{1}{2}(D_a \pm D_b)$, with $C_j = 2t'_j(\frac{1}{3} + u_j^2 - v_j^2)$ and $D_j = 8t'_j/3$. Finally, the wavevector coordinates (q_1, q_2, q_3) are given in terms of the wavevector components of \mathbf{q} by

$$\begin{pmatrix} q_1 \\ q_2 \\ q_3 \end{pmatrix} = \begin{pmatrix} \frac{1}{\sqrt{2}} & -\frac{1}{\sqrt{2}} & 0 \\ \frac{1}{\sqrt{6}} & \frac{1}{\sqrt{6}} & -\frac{2}{\sqrt{3}} \\ \frac{1}{\sqrt{3}} & \frac{1}{\sqrt{3}} & \frac{1}{\sqrt{3}} \end{pmatrix} \begin{pmatrix} q_x \\ q_y \\ q_z \end{pmatrix}.$$

Note that \bar{H}_1 is the specific realization of \bar{H}_b in the main text for the \mathbf{k}_1 point.

Analogous approximate forms for H_{bulk} near the other three L points can be obtained by appropriate symme-

try operations: the states and effective Hamiltonian in the vicinity of $\mathbf{k}_4 \equiv (\frac{\pi}{2}, \frac{\pi}{2}, -\frac{\pi}{2})$ are related to Eqs. S2 and S4 by a mirror reflection across the $x - y$ plane, and these quantities for the other two L points can be constructed by $2\pi/3$ rotations around the (111) direction from those of \mathbf{k}_4 . For example, for the \mathbf{k}_4 point we denote the mirror operation by M_z , and note the fact that $H_{bulk}(k_x, k_y, -k_z) = M_z H_{bulk}(k_x, k_y, k_z) M_z^{-1}$. Writing $\mathbf{k} = \mathbf{k}_4 + \mathbf{q}'$, one finds a long-wavelength form for $H_{bulk}(\mathbf{k})$ in the vicinity of \mathbf{k}_4 , \bar{H}_4 , which is formally the same form as Eq. S4, but with the caveat that the $\tilde{\sigma}_i$ operators act on the mirror reflected states $|1, j\rangle_4 \equiv M_z|1, j\rangle$ and $|2, j\rangle_4 \equiv M_z|2, j\rangle$, and $\mathbf{q} \rightarrow \mathbf{q}'$ with

$$\begin{pmatrix} q'_1 \\ q'_2 \\ q'_3 \end{pmatrix} = \begin{pmatrix} \frac{1}{\sqrt{2}} & -\frac{1}{\sqrt{2}} & 0 \\ \frac{1}{\sqrt{6}} & \frac{1}{\sqrt{6}} & \frac{2}{\sqrt{3}} \\ \frac{1}{\sqrt{3}} & \frac{1}{\sqrt{3}} & -\frac{1}{\sqrt{3}} \end{pmatrix} \begin{pmatrix} q_x \\ q_y \\ q_z \end{pmatrix}.$$

Rewriting \bar{H}_4 in terms of \mathbf{q} , one finds

$$\begin{aligned} \bar{H}_4 = A(\eta q_2 + q_3)\tau_x - B[q_1\tilde{\sigma}'_2 + (q_2 + \eta q_3)\tilde{\sigma}'_1]\tau_y + \left\{ m + C_{12}^{(-)}[q_1^2 + (q_2 + \eta q_3)^2] + C_3^{(-)}(q_2 + \eta q_3)^2 \right\} \tau_z \\ + C_{12}^{(+)}[q_1^2 + (q_2 + \eta q_3)^2] + C_3^{(+)}(q_2 + \eta q_3)^2, \end{aligned} \quad (\text{S5})$$

with $\eta = 2\sqrt{2}/3$. \bar{H}_1 and \bar{H}_4 may be used to construct surface states and effective surface Hamiltonians, as described in the next section.

II. SURFACE HAMILTONIANS

As discussed in the main text, when the mass of the system is negative ($m < 0$) the energy bands described by \bar{H}_1 near the \mathbf{k}_1 point are topological, and we expect that surfaces will host gapless states [2]. These must be eigenstates of \bar{H}_1 , \bar{H}_4 , or of one of the Hamiltonians associated with \mathbf{k}_2 or \mathbf{k}_3 , but with $q_3 \rightarrow i\kappa$, where, in order to satisfy Eq. 2 in the main text, κ must obey

$$(E + C_3^{(+)})^2 = (m - C_3^{(-)}\kappa^2)^2 - A^2\kappa^2. \quad (\text{S6})$$

For a given value of E , one finds two values of κ^2 that satisfy Eq. S6, κ_{\pm}^2 . With the proper choice of overall sign for κ_{\pm} , the eigenstates $|\kappa_{+}\rangle$ and $|\kappa_{-}\rangle$ vanish in real space deep in the bulk of the system, but generically neither vanishes at the surface. However if $|\kappa_{+}\rangle \propto |\kappa_{-}\rangle$,

we can form a linear combination of these that does [3–5]. One may show that for $\text{sgn}(mC_3^{(-)}) < 0$, there is a unique value of E for which this is possible, given by $E = E_{\bar{\Gamma}} \equiv -\frac{C_3^{(+)}}{C_3^{(-)}}m$. Because the states $|\kappa_{\pm}\rangle$ have no dependence on the $\tilde{\sigma}_i$ operators (see Eq. 2 of main text), we can form two independent pairs of these.

The Dirac point states for the \bar{M} points is obtained in a very analogous way. For example, starting with \bar{H}_4 (Eq. S5), we make the replacement $q_3 \rightarrow i\kappa$ and set $q_1 = q_2 = 0$. One may find two different values of κ with the same eigenvectors of \bar{H}_4 at the energy $E_{\bar{M}} = -m\frac{C_{12}^{(+)}\eta^2 + C_3^{(+)}}{C_{12}^{(-)}\eta^2 + C_3^{(-)}}$. Thus we can construct two states meeting the boundary conditions. From the rotational symmetry, each of the other \bar{M} points will host a pair of degenerate states at precisely this energy, yielding three sets of Dirac points. Note that $E_{\bar{M}} \neq E_{\bar{\Gamma}}$, so the Dirac points are at two different energies, in agreement with numerical tight-binding studies [6].

To simplify subsequent discussion, we drop the particle-hole symmetry-breaking terms (i.e., set

$C_{12}^{(+)}, C_3^{(+)} = 0$) in \bar{H}_1 , \bar{H}_4 , and the long-wavelength Hamiltonians for the other L points, except to note that the surface Dirac point energies at the $\bar{\Gamma}$ and \bar{M} points

are different, so that we add $E_{\bar{\Gamma}}$ and $E_{\bar{M}}$ to \bar{H}_1 and \bar{H}_4 , respectively. Thus we make the replacements

$$\begin{aligned}\bar{H}_1 &\rightarrow Aq_3\tau_x - B[q_1\tilde{\sigma}_2 + q_2\tilde{\sigma}_1]\tau_y + [m + C_{12}^{(-)}(q_1^2 + q_2^2) + C_3^{(-)}q_3^2]\tau_z + E_{\bar{\Gamma}}, \\ \bar{H}_4 &\rightarrow A(\eta q_2 + q_3)\tau_x - B[q_1\tilde{\sigma}'_2 + (q_2 + \eta q_3)\tilde{\sigma}'_1]\tau_y + \left\{m + C_{12}^{(-)}[q_1^2 + (q_2 + \eta q_3)^2] + C_3^{(-)}(q_2 + \eta q_3)^2\right\}\tau_z + E_{\bar{M}}.\end{aligned}\tag{S7}$$

These Hamiltonians are next projected into space of surface states derived above. The explicit form of these that are relevant for the $\bar{\Gamma}$ point (with effective Hamiltonian \bar{H}_1) are

$$\begin{aligned}|u_1\rangle &= \frac{1}{\sqrt{2}} \begin{pmatrix} 1 \\ 0 \\ -i\text{sgn}(A) \\ 0 \end{pmatrix} \mathcal{N}_z (e^{-\kappa_+ z} - e^{-\kappa_- z}), \\ |u_2\rangle &= \frac{1}{\sqrt{2}} \begin{pmatrix} 0 \\ 1 \\ 0 \\ -i\text{sgn}(A) \end{pmatrix} \mathcal{N}_z (e^{-\kappa_+ z} - e^{-\kappa_- z}).\end{aligned}$$

In these expressions, the four entries are coefficients of the $(|1, a\rangle, |2, a\rangle, |1, b\rangle, |2, b\rangle)$ states at the \mathbf{k}_1 point, z denotes the direction perpendicular to the surface (with $z > 0$ being points inside the system), \mathcal{N}_z is a normalization constant, and $\kappa_{\pm}^2 = m + [A^2 \pm \sqrt{4mC_3^{(-)}A^2 + A^4}]/2C_3^{(-)}$. Note that the wavefunctions have equal weight on the two sublattices, and moreover are eigenstates of the $\tilde{\sigma}_3$ operator. The corresponding results for the \mathbf{k}_4 point may also be written as eigenstates of the relevant $\tilde{\sigma}_3$ operator (i.e., acting on states near the \mathbf{k}_4 point), and also have equal weight on the two sublattices, although the relative phase is more complicated and has the form

$$e^{i\theta_4} \equiv \frac{A - i\eta B}{\sqrt{A^2 + \eta^2 B^2}}.$$

With the explicit surface wavefunctions in hand it is straightforward to project \bar{H}_1 and \bar{H}_4 onto the space of surface states, yielding surface Hamiltonians for the $\bar{\Gamma}$ and \bar{M} points. These take the form

$$H_{\bar{\Gamma}} \equiv B[q_1\tilde{\sigma}_2 + q_2\tilde{\sigma}_1] + E_{\bar{\Gamma}}\tag{S8}$$

and

$$H_{\bar{M}} \equiv \frac{AB}{\sqrt{A^2 + \eta^2 B^2}} [(\eta^2 - 1)q_2\tilde{\sigma}_1 + q_1\tilde{\sigma}_2] + E_{\bar{M}}.\tag{S9}$$

Note that the states which the $\tilde{\sigma}_i$ operators act upon in $H_{\bar{M}}$ are different than those of $H_{\bar{\Gamma}}$. Analogous results may be obtained for the other two \bar{M} points by $2\pi/3$ rotations of Eq. S9.

As described in the main text, we assume that there are impurity spins which order ferromagnetically on the surface, and treat these in mean-field theory, so that they form an effective uniform Zeeman field that couples to the electron spin operators, projected onto the surface states, as shown in Eq. 3 in the main text. Adding these to the various Hamiltonians (e.g., Eqs. S8 and S9) leads to the generic Hamiltonian in Eq. 4 of the main text.

III. SPIN STIFFNESS COEFFICIENTS

In this section, we describe our computation of the spin stiffness for a fully filled band. For simplicity we consider an isotropic surface Dirac cone, as is found for the $\bar{\Gamma}$ point; anisotropic Dirac cones (\bar{M} points) should yield qualitatively similar results. Our generic Hamiltonian has the form

$$H_0 = \alpha [(q_x + b_x)\sigma_x + (q_y + b_y)\sigma_y + b_z\sigma_z],$$

where for simplicity of notation we have rewritten the parameter Δ_i in the text as αb_z . Eigenstates of H_0 are spinors of the form

$$\begin{pmatrix} u \\ v \end{pmatrix}_p = \frac{e^{i\mathbf{q}\cdot\mathbf{r}}}{\mathcal{S}^{1/2}\sqrt{q'^2 + (p\varepsilon_0(\mathbf{q}) - b_z)^2}} \begin{pmatrix} q'_x - iq'_y \\ p\varepsilon_0(\mathbf{q}) - b_z \end{pmatrix} \equiv |\mathbf{q}, p\rangle,$$

where $p = \pm 1$ is the band index for states with energy $p\varepsilon(\mathbf{q}) = p\sqrt{q_x'^2 + q_y'^2 + b_z^2}$, $(q'_x, q'_y) = (q_x + b_x, q_y + b_y)$, and \mathcal{S} is the area of the surface. We consider the effect on the total electronic energy of a filled lower band ($p = -1$) of

adding a spatially varying component to \mathbf{b} , of the form $h = \delta \vec{b} \cdot \vec{\sigma} \cos \mathbf{Q} \cdot \mathbf{r}$ to H_0 , focusing on its dependence on

\mathbf{Q} for small Q . Using second order perturbation theory, one finds for the energy shift $\delta E(\mathbf{Q})$ that

$$\begin{aligned} \delta E(\mathbf{Q}) - \delta E(0) &\approx \frac{1}{32} \sum_{\mu, \nu=x,y} Q_\mu Q_\nu \sum_{\mathbf{q}} \left\{ \frac{|\langle \mathbf{q}, -1 | \delta \vec{b} \cdot \vec{\sigma} | \mathbf{q}, +1 \rangle|^2}{\varepsilon_0(\mathbf{q})^2} \partial_\mu \partial_\nu \varepsilon_0(\mathbf{q}) - \frac{1}{\varepsilon_0(\mathbf{q})} \partial_\mu \partial_\nu |\langle \mathbf{q}, -1 | \delta \vec{b} \cdot \vec{\sigma} | \mathbf{q}, +1 \rangle|^2 \right\} \\ &\equiv \frac{\mathcal{S}}{2} \sum_{\mu, \nu=x,y} \rho_{\mu, \nu} Q_\mu Q_\nu. \end{aligned} \quad (\text{S10})$$

With a lengthy albeit in principle straightforward calculation, the coefficients $\rho_{\mu, \nu}$ may all be computed explicitly, with the results

$$\begin{aligned} \rho_{xx} &= \frac{2}{\pi \Delta^{(0)}} \left[\frac{2}{5} \alpha^2 \delta b_x^2 + \frac{8}{15} \alpha^2 \delta b_y^2 + \frac{4}{15} \alpha^2 \delta b_z^2 \right], \\ \rho_{yy} &= \frac{2}{\pi \Delta^{(0)}} \left[\frac{8}{15} \alpha^2 \delta b_x^2 + \frac{2}{5} \alpha^2 \delta b_y^2 + \frac{4}{15} \alpha^2 \delta b_z^2 \right], \\ \rho_{xy} &= \frac{2}{\pi \Delta^{(0)}} \left[\frac{8}{15} \alpha^2 \delta b_x \delta b_y \right], \end{aligned}$$

where $\Delta^{(0)} = \alpha b_z$ is the gap for the unperturbed spectrum of H_0 .

-
- [1] T. Hsieh, H. Lin, J. Liu, W. Duan, and L. Fu, Nat. Commun. **3**, 982 (2012).
 - [2] J. Liu, W. Duan, and L. Fu, Phys. Rev. B **88**, 241303(R) (2013).
 - [3] C.-X. Liu, X.-L. Qi, H. Zhang, X. Dai, Z. Fang, and S.-C. Zhang, Phys. Rev. B **82**, 045122 (2010), URL <https://link.aps.org/doi/10.1103/PhysRevB.82.045122>.
 - [4] P. G. Silvestrov, P. W. Brouwer, and E. G. Mishchenko, Phys. Rev. B **86**, 075302 (2012), URL <http://link.aps.org/doi/10.1103/PhysRevB.86.075302>.
 - [5] L. Brey and H. A. Fertig, Phys. Rev. B **89**, 084305 (2014).
 - [6] C. Polley and et al., Phys. Rev. B **89**, 075317 (2014).